hep/ph-0703040
STUPP-07-189

An illustration and analysis of the degeneracy in the search for the leptonic CP-violating angle and the neutrino mass hierarchy

Masafumi Koike[1,*] and Masako Saito[1,†]

[1] *Physics Department, Saitama University, 255 Shimo-Okubo, Sakura-ku, Saitama, Saitama 338-8570, Japan*

(Dated: March 6, 2007)

Determination of the value of the leptonic CP-violating angle δ and the neutrino mass hierarchy $\mathrm{sgn}\,\delta m^2_{31}$ through long baseline neutrino oscillation experiments is systematically analyzed. We note that the two oscillation spectra are difficult to discriminate and lead to the degeneracy when they are peaked at the same energy and have the same peak probability. The condition of peak-matching is thereby introduced as a criterion of the presence of degeneracy. Matching of peaks is visualized as an intersection of trajectories traced by a peak of an oscillation spectrum while the value of δ is varied from 0 to 2π. We numerically calculate a pair of trajectories for a pair of hierarchies and examine the degeneracy, especially the one on the hierarchy. We formulate the trajectory into analytic expressions and give an evaluation of the critical length, which is shown to be proportional to $1/\sin\theta_{13}$. We take the following four approaches to solving the hierarchy degeneracy and provide prospects in view of our analysis: elongating the baseline length sufficiently, using both neutrinos and anti-neutrinos, combining experiments with different baseline lengths, and observing two or more oscillation peaks.

PACS numbers: 14.60.Pq, 11.30.Er, 13.15.+g, 14.60.Lm

I. INTRODUCTION

Experiments suggest the oscillation among the different flavors of neutrinos, providing rich information on the flavor structure of the lepton sector [1, 2, 3, 4]. Present knowledge of neutrinos is nevertheless still incomplete and awaits the improvement. In the notations of Ref. [5], the values of the mass parameters and the mixing parameters yet to be known include one of the mixing angles θ_{13}, the sign of δm^2_{31}, and the CP-violating angle δ. The value of θ_{13} is confined only by an upper bound as $\sin^2 2\theta_{13} < 0.19$ [5], while the sign of δm^2_{31} and the value of δ are completely unknown to date. The CP violation manifests itself only in the flavor-changing appearance channel such as $\nu_\mu \to \nu_\mathrm{e}$, which in turn is suppressed by a small factor of $\sin^2 2\theta_{13}$. On this account, we expect the two-staged strategy in pursuing the unknown natures of neutrinos. The first stage is the search for θ_{13}. Its upper bound is anticipated to be improved down to $\sin^2 2\theta_{13} \lesssim O(10^{-2})$ by planned experiments using nuclear reactors [6] and accelerators [7]. The second stage is the search for the sign of δm^2_{31} and for the CP violation. The next generations of long baseline neutrino oscillation experiments will offer promising opportunities for the searches [7].

Our focus in this paper is on the second stage based on an optimistic expectation that next-generation reactor neutrino experiments will find evidences of non-vanishing θ_{13} and that its value will be proven large enough for the CP-violation search. We consider the search for the CP-violating angle through long baseline neutrino oscillation experiments using a conventional beam of muon neutrinos. Since the search for δ is entangled with that for the sign of δm^2_{31}, the values of these two are not necessarily determined uniquely by a single experiment with a fixed baseline length, and can be left degenerate. The parameter degeneracy obstructs an efficient search for the parameter values and should be avoided [8, 9, 10, 11]. Its presence is, however, difficult to predict comprehensively due to the complicated dependence of experimental results upon many parameters and controllable setups of experiments. The plot introduced in Ref. [10] gives an overview of the presence of degeneracy and has been found versatile for its analysis. It presents the two oscillation probabilities or event rates of two channels on a two-dimensional space, enabling to show separately the CP-violating effect and the matter effect.

We introduce another aspect of the analysis of the appearance spectrum. Giving an intuitive illustration on the determination of the parameters from the spectrum, we offer a view of ours on the emergence of degeneracy and its resolution. The pivot of our study is the peak of the oscillation probability, especially its position, or the energy and probability at the peak. We note that two oscillation spectra whose peak positions coincide are difficult to distinguish and likely to cause the degeneracy. We trace the peak position varying the values of δ and $\mathrm{sgn}\,\delta m^2_{31}$ to show how the search for them is entangled and the degeneracy is invited. We change the baseline length as well and describe from our point of view how the degeneracy disappears when the baseline gets long. We organize these analyses by deriving analytic expressions of the oscillation probability at the peaks and offer an outlook of the presence of degeneracy and possible ways to avoid it.

The outline of this paper is as follows. In Sec. II, we introduce the peak-matching condition as a criterion for

*Electronic address: koike@krishna.th.phy.saitama-u.ac.jp
†Electronic address: msaito@krishna.th.phy.saitama-u.ac.jp

the presence of degeneracy and visualize it by drawing closed trajectories of the oscillation peak. In Sec. III, we develop an understanding of the presence and absence of the degeneracy of parameters through the loops of the peak. In Sec. IV, we derive an analytic expression for the $\nu_\mu \to \nu_e$ appearance probability at the oscillation peaks to elucidate its dependence on the mass parameters and the mixing parameters, and show how the loops are distorted due to the change of the baseline length. In Sec. V, we apply the peak loops to the evaluation of four methods to determine uniquely the value of CP-violating angle and the mass hierarchy. Section VI presents the conclusion and discussions.

II. PEAK-MATCHING CONDITION AND THE PEAK LOOP

We assume that the number of neutrino generations is three and adopt the definitions given in Ref. [5] of the quadratic mass differences δm^2_{ij} ($\{i,j\} \subset \{1,2,3\}$), the mixing angles θ_{ij}, and the CP-violating angle δ. All the experiments carried out so far can be attributed to the neutrino oscillation by taking $\delta m^2_{21} \simeq (8.0^{+0.4}_{-0.3}) \times 10^{-5}\,\mathrm{eV}^2$, $|\delta m^2_{31}| \simeq (1.9\text{–}3.0) \times 10^{-3}\,\mathrm{eV}^2$, $\sin^2 2\theta_{12} = 0.86^{+0.03}_{-0.04}$, $\sin^2 2\theta_{23} > 0.92$, and $\sin^2 2\theta_{13} < 0.19$ [5] with an exception of the LSND experiment [12]. We do not take account of ambiguities of these parameters in this paper for a clear presentation of our idea. The influence of their ambiguities will be discussed in Sec. VI.

We consider the search for the CP-violating angle δ and the mass hierarchy $\mathrm{sgn}\,\delta m^2_{31}$ by observing $\nu_\mu \to \nu_e$ appearance probability in long baseline neutrino oscillation experiments. We do not deal with the disappearance channel, which is effective in practical analyses to restrict parameter values such as the absolute value of δm^2_{31}. Let us illustrate with an example that $\nu_\mu \to \nu_e$ appearance probability enables the pursuit of the value of δ and sign of δm^2_{31}. We show in Fig. 1 the $\nu_\mu \to \nu_e$ appearance probabilities for baseline length $L = 700\,\mathrm{km}$. The value of δ and the sign of δm^2_{31} are varied while other parameters are fixed to a set of example values:

$$\delta m^2_{21} = 8.2 \times 10^{-5}\,\mathrm{eV}^2\,, \tag{1a}$$

$$\left|\delta m^2_{31}\right| = 2.5 \times 10^{-3}\,\mathrm{eV}^2\,, \tag{1b}$$

$$\sin^2 2\theta_{12} = 0.84\,, \tag{1c}$$

$$\sin^2 2\theta_{23} = 1.0\,, \tag{1d}$$

$$\sin^2 2\theta_{13} = 0.06\,. \tag{1e}$$

The matter density ρ on the baseline is assumed to be constant and fixed to

$$\rho = 2.6\,\mathrm{g/cm}^3, \tag{1f}$$

which is related to the electron number density n_e as $n_e = N_A Y_e \rho$ with the Avogadro number N_A and the proton-to-nucleon ratio Y_e on the baseline. We conveniently use this example set of values and assume

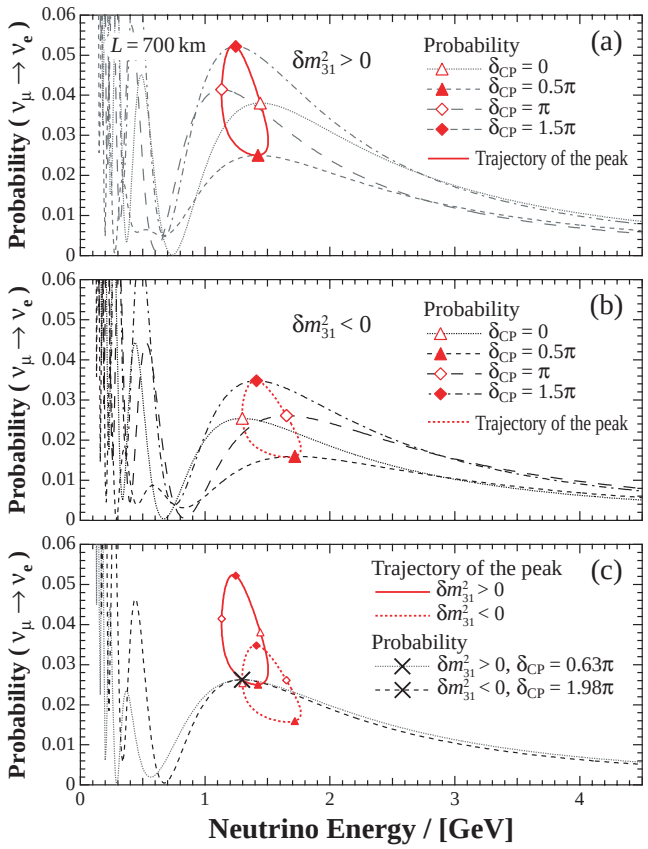

FIG. 1: (Color online) The $\nu_\mu \to \nu_e$ appearance probabilities and the trajectories of their first peaks for the baseline length of 700 km. The oscillation parameters in Eq. (1) are adopted. The top figure (a) is for the normal hierarchy and the middle (b) for the inverted, and each includes the probability spectra for $\delta = 0, \pi/2, \pi$ and $3\pi/2$. The bottom figure (c) reproduces the trajectories in (a) and (b) overlaid, along with two oscillation spectra peaked at the crossed intersection of these trajectories.

$Y_e = 0.5$ for the numerical calculations in this paper unless otherwise noticed. Figure 1 shows the energy spectra of the appearance probability (a) for $\delta m^2_{31} = +2.5 \times 10^{-3}\,\mathrm{eV}^2 > 0$ (normal hierarchy) and (b) for $\delta m^2_{31} = -2.5 \times 10^{-3}\,\mathrm{eV}^2 < 0$ (inverted hierarchy). Figure 1 (c) displays two spectra for the set of parameter values given in it. We can clearly see the dependence of the spectrum upon δ and $\mathrm{sgn}\,\delta m^2_{31}$ in (a) and (b), and thus we can search for these values through $\nu_\mu \to \nu_e$ appearance experiments.

This dependence, however, does not guarantee that we can uniquely determine these values from an experiment. Experimental results in some cases are consistent with both normal and inverted hierarchy, each with an appropriate choice of the value of δ. For example, an experiment providing the oscillation spectrum of the dashed line in Fig. 1 (c) would reject neither $(\mathrm{sgn}\,\delta m^2_{31}, \delta) = (+, 0.63\pi)$ nor $(\mathrm{sgn}\,\delta m^2_{31}, \delta) = (-, 1.98\pi)$

if the low-energy neutrinos below about 1 GeV are unobservable. We refer to this uncertainty as hierarchy degeneracy, which is a case of parameter degeneracy considered in the literatures [8, 9, 10]. The presence of degeneracy is an unfavorable complication of the analysis and should be avoided.

We direct our attention to the peak of the appearance probability spectrum as it turns out to give an insight into the presence of hierarchy degeneracy. An appearance probability has a series of peaks $(E_{\mathrm{peak},n}, P_{\mathrm{peak},n})$ $(n = 0, 1, 2, \cdots)$ with $E_{\mathrm{peak},0} > E_{\mathrm{peak},1} > E_{\mathrm{peak},2} > \cdots$. Each peak makes a trajectory of a closed loop as we vary the value of δ from 0 to 2π keeping other parameters fixed. The loops drawn by the first peak ($n = 0$) are presented in Fig. 1 (a) for $\delta m^2_{31} > 0$ and (b) for $\delta m^2_{31} < 0$. The peak positions for $\delta = 0$, $\pi/2$, π, and $3\pi/2$ are indicated on the loops by open triangles, solid triangles, open diamonds, and solid diamonds, respectively. We observe that the peak position for the normal (inverted) hierarchy moves clockwise (counterclockwise) on the loop as the value of δ increases.

In Fig. 1 (c), the peak loops for $\delta m^2_{31} \gtrless 0$ are copied from Figs. 1 (a) and (b) with a cross marked on one of their intersections. The intersection corresponds to two sets of parameter values given in the figure. These values give the shown oscillation probabilities both peaked at the cross as they should. We observe the noticeable similarity of the two for $E \gtrsim 1\,\mathrm{GeV}$ despite the difference in the energy below. Given the typical visible energy $E > (0.5-1.0)\,\mathrm{GeV}$ of neutrinos, we expect that their similarity makes it difficult to distinguish the two sets of parameter values by experiments and thus lead to the degeneracy.

We arrive here at an intuitive view of the presence of the degeneracy. Assume that the visible energy range of the experiment covers only one peak $(E_{\mathrm{peak},n}, P_{\mathrm{peak},n})$ of the appearance probability; we discuss later the cases where more than one peaks are visible, which occurs for a sufficiently long baseline length (typically $L \gtrsim 1000\,\mathrm{km}$). The values of $E_{\mathrm{peak},n}$ and $P_{\mathrm{peak},n}$ depend on oscillation parameters such as δm^2_{ij}, θ_{ij}, and δ, which we collectively denote by $\{\vartheta_i\}$. Our observation in the previous paragraph signifies that the two parameter sets $\{\vartheta_i\}$ and $\{\vartheta'_i\}$ are expected to be degenerate when the peak-matching condition

$$E_{\mathrm{peak},n}\big(\{\vartheta_i\}\big) = E_{\mathrm{peak},n}\big(\{\vartheta'_i\}\big)\,, \tag{2a}$$

$$P_{\mathrm{peak},n}\big(\{\vartheta_i\}\big) = P_{\mathrm{peak},n}\big(\{\vartheta'_i\}\big) \tag{2b}$$

is satisfied. This condition was first put to the test in Ref. [13] in the analysis of an example study, although not extensively. The hierarchy degeneracy in particular arises when the values of δm^2_{31} in $\{\vartheta_i\}$ and in $\{\vartheta'_i\}$ have the opposite signs.

We confirm the intuitive discussion above by a quantitative comparison of the two spectra shown in Fig. 1 (c), following the analysis carried out in Sec. III A of Ref. [13]. The assumed experimental setups and included backgrounds are the same as in this reference except for the baseline length which is set to 700 km here. The analysis is briefly outlined as follows. We fix the set of "true" parameter values as $(\delta m^2_{31}, \delta) = (+2.5\times10^{-3}\,\mathrm{eV}^2, 0.63\pi)$ taken from Fig. 1 (c), along with the values in Eq. (1). Opposed is that of "test" values which are varied over the δ-δm^2_{31} parameter space with other parameters fixed to the true values. We generate an energy spectrum for this test value and check its consistency to the true value via a χ^2 goodness-of-fit analysis. The test values that pass this check constitute the allowed region. Figure 2 shows the allowed region of 68.3% and 95% confidence levels obtained from the χ^2 analysis over $0.7\,\mathrm{GeV} < E < 3.1\,\mathrm{GeV}$. The top graph is for the normal hierarchy, and the bottom for the inverted. The large cross on the top graph indicates the true values of parameters, and the allowed region extends around the cross due to statistical error, systematic error, and backgrounds. Also in the bottom graph is the allowed region, which implies the presence of the hierarchy degeneracy. The small cross marked at $(\delta m^2_{31}, \delta) = (-2.5\times10^{-3}\,\mathrm{eV}^2, -0.02\pi)$ indicates the peak-matching partner of the true value of our choice shown in Fig. 1 (c) as $-0.02\pi \equiv 1.98\pi \bmod 2\pi$. Note that it falls just within the allowed region with the wrong hierarchy, indicating the degeneracy of the two sets of parameter values.

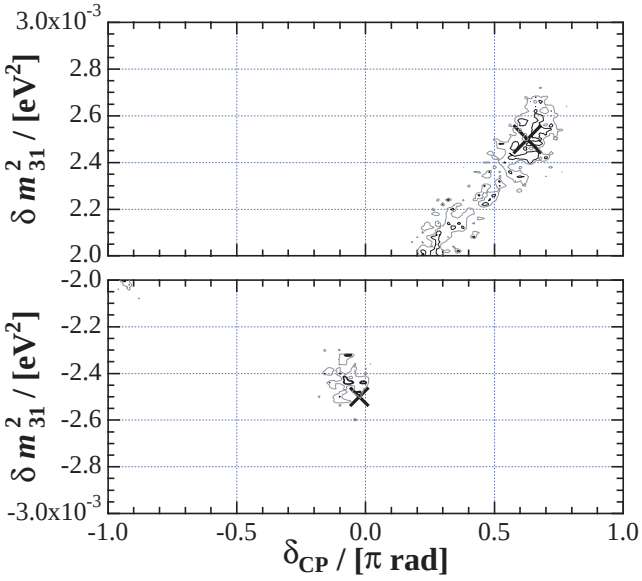

FIG. 2: Allowed regions for 68.3% (gray line) and 95% (black line) confidence levels obtained from an example χ^2 analysis of the $\nu_\mu \to \nu_\mathrm{e}$ appearance events between 0.7 GeV and 3.1 GeV. The large cross on the top figure denotes the true values of parameters of our choice and the small one on the bottom shows the peak-matching partner of the true values as explained in the text.

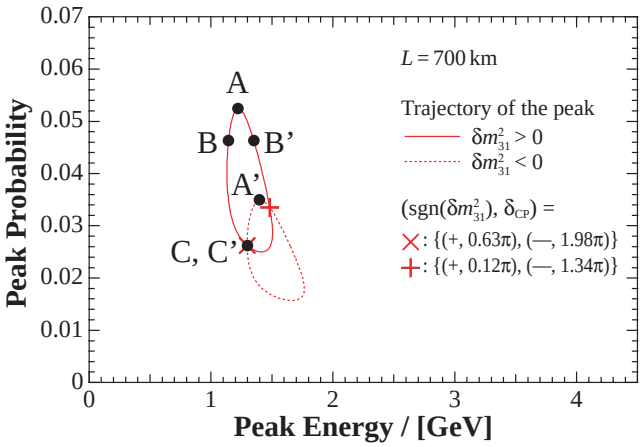

FIG. 3: (Color online) Trajectories of the first oscillation peak for the baseline length of 700 km. The oscillation parameters in Eq. (1) are adopted. The solid line is for the normal hierarchy and the dotted one for the inverted. A cross and a plus sign denote the intersections of the trajectories. The points of A, A′, B, B′, C, and C′ are referred to in the text.

III. DEGENERACY IN LIGHT OF THE PEAK LOOPS

We have shown in the previous section that the degeneracy follows from the two parameter sets which bring the oscillation peak to the same position. We employ the peak loops in this section to present a simple understanding of the presence of the degeneracy.

A. Emergence of the degeneracy: case studies

We explain how we can read the presence and absence of the hierarchy degeneracy from the peak loops introduced in the previous section. In Fig. 3, we reproduce the pair of peak loops presented in Fig. 1 (c). The upper loop for $\delta m^2_{31} > 0$ and the lower loop for $\delta m^2_{31} < 0$ intersect at two points, each of which gives a pair of the values of $(\mathrm{sgn}\,\delta m^2_{31}, \delta)$; in this example the two pairs are

$$\left\{(+, 0.63\pi)\,, (-, 1.98\pi)\right\}, \tag{3a}$$
$$\left\{(+, 0.12\pi)\,, (-, 1.34\pi)\right\}. \tag{3b}$$

The true values of $(\mathrm{sgn}\,\delta m^2_{31}, \delta)$ provided by the Nature give an oscillation spectrum whose first peak falls on some point on the two loops. We can correctly determine these values by identifying the point through experiments. Sufficient precision and accuracy are necessary to put it into practice. Even an well-controlled experiment, however, fails to determine uniquely the parameter values if the true peak falls right upon an intersection of the loops, giving two possible sets of values as seen in Eq. (3). We demonstrate how degeneracies emerge for three typical cases where the true peak is at the points A, B, and C in Fig. 3.

Case (A): the true hierarchy is normal and the true oscillation peak is at the point A in Fig. 3. Owing to the vertical separation of the two loops, the sign of δm^2_{31} is determined as positive once the appearance probability is determined well enough to distinguish the point A from the point A′. The value of δ is restricted in a single allowed region around the value for A and the extent of the region depends on the experimental precision and accuracy.

Case (B): the true hierarchy is normal and the true oscillation peak is at the point B in Fig. 3. The value of δ is constrained in a single allowed region as in the previous case if the energy resolution of the experiment is high enough to distinguish the points B and B′ on the paralleling sides of the loop. If, on the other hand, the resolution is not enough, the value of δ for B and for B′ become degenerate and the allowed region will extend around these two values.

Case (C): the true hierarchy is normal, and the true oscillation peak is at the point C which is the intersection of the two loops. There exists another value of δ that brings the oscillation peak at the same point C′ but with the inverted hierarchy, and we are led to the hierarchy degeneracy. Here we regard the points C and C′ are on the upper and the lower loop, respectively, in spite of their coincidence in the position. The allowed region consists of two separate parts which extend around the parameters for C and for C′.

B. Degeneracy in varying the baseline length

Next we examine how a pair of loops move and get distorted as we vary the baseline length of the neutrino oscillation experiments. We present in Fig. 4 peak loops varying the baseline length from 300 km to 1500 km while fixing other parameters to the example value of Eq. (1). For a relatively short baseline ($L \sim 300$km for our example), the loop for the normal hierarchy ("normal loop") and for the inverted hierarchy ("inverted loop") have similar shape and lie largely overlapped with each other. As the baseline becomes longer, the normal loop and the inverted loop move upward and downward, respectively, and diverge due to the matter effect. The inverted loop is at the same time appreciably stretched in the E-direction and flattened in the P-direction. The two loops are seen to become disjoint at a certain baseline length. This critical length $L_{\rm crit}$ for present parameter set is $L_{\rm crit} \simeq (1100 - 1300)$ km as can be read in Fig. 4.

We reach following outlooks upon determining the hierarchy and the CP-violating angle from the above observations.

The hierarchy is difficult to determine by experiments with a short baseline length where the pair of loops overlaps considerably. We expect, however, that the hierarchy can be determined when the true peak lies at the

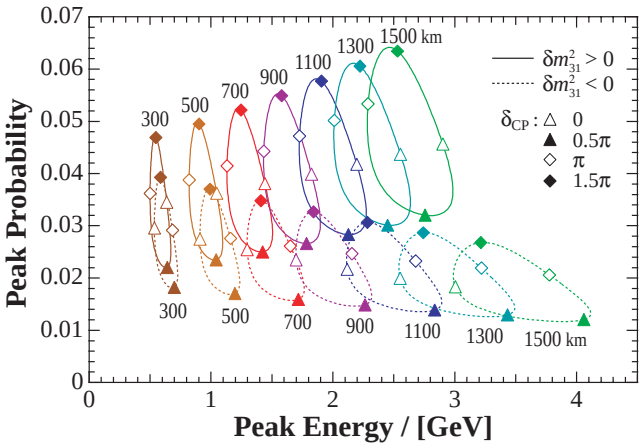

FIG. 4: (Color online) Trajectories of the first oscillation peak for the baseline lengths between 300 km and 1500 km. The oscillation parameters in Eq. (1) are adopted. The solid line is for the normal hierarchy and the dotted one for the inverted.

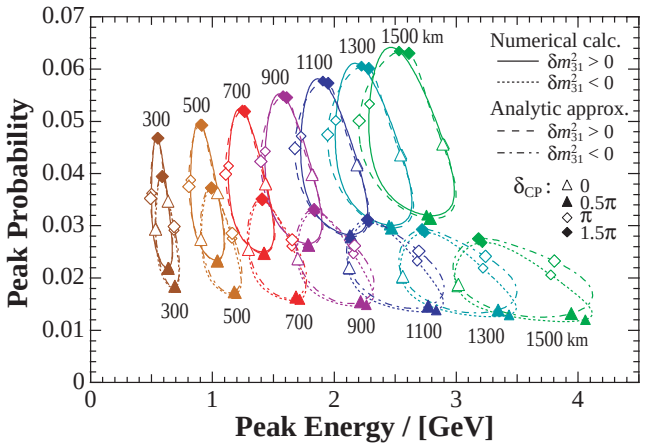

FIG. 5: (Color online) Trajectories of the first oscillation peak for the baseline lengths between 300 km and 1500 km obtained from the numerical calculation (the solid line for the normal hierarchy and the dotted for the inverted) and analytic approximations (the dashed line for the normal hierarchy and the dash-dotted for the inverted). The oscillation parameters in Eq. (1) are adopted.

top part of the upper loop or at the bottom part of the lower loop. The determination of the hierarchy becomes easier as the baseline becomes longer and the increasing effect of the matter separates the pair of loops. When the baseline is longer than the critical length, the condition of Eq. (2) is never satisfied with opposite hierarchies and the hierarchy is thus uniquely determined regardless of the value of δ.

The search for the value of δ is entangled with that for the hierarchy. The hierarchy degeneracy is one obstacle to the determination of the value of δ especially when the baseline is short. Another obstacle is the experimental limitation on the energy resolution and on the precision and the accuracy of the oscillation probability. The loop is narrow in the E-direction when the baseline is short, and the resolution of the energy needs to be high enough to distinguish the paralleling sides of the loops; otherwise an additional degeneracy will be invited. In contrast, the inverted loop is flattened in the P-direction when the baseline length is long. We thus require precise and accurate measurements of the oscillation probability to avoid introducing an extra degeneracy.

IV. ANALYTIC STUDY OF THE PEAK LOOPS

We have illustrated the determination of parameters with the aid of peak loops and found their position, size, and shape informative. In this section, we exploit analytic expressions of the oscillation probability to formulate them in terms of the mass parameters, the mixing parameters, and the baseline length. We thereby analyze how a pair of peak loops for $\delta m^2_{31} \gtrless 0$ are distorted and separated as the baseline length increases.

A. Formulation of the peak loops via the oscillation probability formula

We derive formulae of the oscillation probability by the perturbative expansion of the S-matrix in terms of $\Delta_{21} \equiv \delta m^2_{21} L/2E$ and $\Delta_{\rm m} \equiv \sqrt{2} G_{\rm F} n_{\rm e} L$, where $G_{\rm F} = 1.166 \times 10^{-5}\,{\rm GeV}^{-2}$ is the Fermi constant. The derivation was first worked out to the first order to analyze the effect of CP violation separately from the matter effect [14]. In the present paper, we calculate the $\nu_\mu \to \nu_{\rm e}$ appearance probability to the second order for the following consideration. Note that a peak loop collapses to a point when δm^2_{21} vanishes since the CP violation is a three-generation effect. The size of the peak loop is thus of the first order, and its distortion depending on the baseline length, which we are interested in, is of the second order or higher. The second-order calculation outlined in Appendix A results in lengthy expressions and we apply an additional simplification considering the smallness of θ_{13}. We drop $O(\sin^2\theta_{13})$-terms in the coefficients of Δ^2_{21} and $\Delta_{\rm m}\Delta_{21}$ as well as $O(\sin^3\theta_{13})$-terms in that of $\Delta^2_{\rm m}$. Here we take account of $\Delta_{\rm m} > \Delta_{21}$, which holds for the cases we are interested in (see Appendix B). We then obtain

$$P(\nu_\mu \to \nu_{\rm e}, E) = 4l(A \sin^2\Theta + B)\,, \tag{4a}$$

where

$$\begin{aligned} A = {} & 1 + 2\frac{\Delta_{\rm m}}{\Delta_{31}}(1 - 2s^2_{13}) - \Delta_{21}\frac{j}{l}\sin\delta \\ & - \Delta_{21}\frac{\Delta_{\rm m}}{\Delta_{31}}\frac{j}{l}\left(\sin\delta + \frac{\Delta_{31}}{2}\cos\delta\right) \\ & + \frac{\Delta^2_{21}}{2}\frac{j}{l}\left[\frac{j}{l}\cos\delta + (1 - 2s^2_{12})\right]\cos\delta + 3\frac{\Delta^2_{\rm m}}{\Delta^2_{31}}\,, \end{aligned} \tag{4b}$$

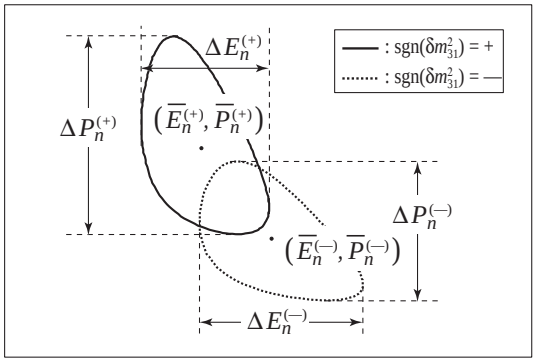

FIG. 6: Notations to designate the central position, the width, and the height of the trajectories of the $(n+1)$-th oscillation peak.

Here

$$l = c_{13}^2 s_{13}^2 s_{23}^2 \,, \tag{5}$$

$$j = c_{13}^2 s_{13} c_{23} s_{23} c_{12} s_{12} \,, \tag{6}$$

$\Delta_{ij} = \delta m_{ij}^2 L/2E$, $s_{ij} = \sin\theta_{ij}$, and $c_{ij} = \cos\theta_{ij}$. The approximation we employed in deriving Eq. (4) is suitable especially for a short baseline, typically for $L < O(10^3\,\mathrm{km})$; see Appendix B. The oscillation probability for anti-neutrinos $P(\bar{\nu}_\mu \to \bar{\nu}_\mathrm{e}, E)$ is obtained by changing the sign of δ and Δ_m.

$$\begin{aligned}\Theta = {} & \frac{\Delta_{31}}{2} - \frac{\Delta_\mathrm{m}}{2}(1-2s_{13}^2) + \frac{\Delta_{21}}{2}\Big(\frac{j}{l}\cos\delta - s_{12}^2\Big) \\ & - \frac{\Delta_{21}}{2}\frac{\Delta_\mathrm{m}}{\Delta_{31}}\frac{j}{l}\Big(\cos\delta + \frac{\Delta_{31}}{2}\sin\delta\Big) \\ & + \frac{\Delta_{21}^2}{2}\frac{j}{l}\left[\frac{j}{l}\cos\delta + \frac{1}{2}(1-2s_{12}^2)\right]\sin\delta \,,\end{aligned} \tag{4c}$$

and

$$B = \frac{\Delta_{21}^2}{4}\frac{j^2}{l^2}\sin^2\delta \,. \tag{4d}$$

We obtain the peak energy which gives the local maxima of the oscillation probability of Eq. (4) as

$$\begin{aligned}E_{\mathrm{peak},n} = \frac{|\delta m_{31}^2|L}{2\Pi}\Bigg\{ & \left[1 \mp \Delta_\mathrm{m}\frac{1}{\Pi}\Big(1-\frac{4}{\Pi^2}\Big)(1-2s_{13}^2) \mp Rs_{12}^2 + \Delta_\mathrm{m}^2\frac{1}{\Pi^2}\Big(1-\frac{12}{\Pi^2}+\frac{48}{\Pi^4}\Big) - R^2\frac{1}{2}\Big(1-\frac{4}{\Pi^2}\Big)\frac{j^2}{l^2}\right] \\ & + R\left[\pm 1 - \Delta_\mathrm{m}\frac{1}{\Pi}\Big(1-\frac{8}{\Pi^2}\Big) - 2R(1-2s_{12}^2)\right]\frac{j}{l}\cos\delta \\ & + R\frac{2}{\Pi}\left[1 \mp \Delta_\mathrm{m}\frac{\Pi}{4}\Big(1+\frac{8}{\Pi^2}-\frac{64}{\Pi^4}\Big) \pm R\frac{\Pi^2}{4}(1-2s_{12}^2)\right]\frac{j}{l}\sin\delta \\ & - R^2\frac{3}{2}\Big(1+\frac{4}{3}\frac{1}{\Pi^2}\Big)\frac{j^2}{l^2}\cos 2\delta \pm R^2\frac{\Pi}{2}\frac{j^2}{l^2}\sin 2\delta\Bigg\} \,,\end{aligned} \tag{7}$$

where $n = 0, 1, 2, \cdots$ is the peak index, $\Pi \equiv (2n+1)\pi$, $R \equiv \delta m_{21}^2/|\delta m_{31}^2|$, and the top of the double sign is for $\delta m_{31}^2 > 0$ and the bottom for $\delta m_{31}^2 < 0$. The oscillation probability at the peak energy is given by

$$\begin{aligned}P_{\mathrm{peak},n} = 4l\Bigg\{ & \left[1 \pm \Delta_\mathrm{m}\frac{2}{\Pi}(1-2s_{13}^2) + R^2\frac{3}{8}\Pi^2\Big(1+\frac{4}{3}\frac{1}{\Pi^2}\Big)\frac{j^2}{l^2} + \Delta_\mathrm{m}^2\frac{1}{\Pi^2}\Big(1+\frac{4}{\Pi^2}\Big)\right] \\ & - R\frac{\Pi^2}{2}\left[\Delta_\mathrm{m}\frac{1}{\Pi}\Big(1-\frac{4}{\Pi^2}\Big) - R(1-2s_{12}^2)\right]\frac{j}{l}\cos\delta - R\Pi\left[1 \pm \Delta_\mathrm{m}\frac{2}{\Pi}\Big(1-\frac{2}{\Pi^2}\Big) \pm Rs_{12}^2\right]\frac{j}{l}\sin\delta \\ & + R^2\frac{\Pi^2}{8}\Big(1-\frac{4}{\Pi^2}\Big)\frac{j^2}{l^2}\cos 2\delta \pm R^2\frac{\Pi}{2}\frac{j^2}{l^2}\sin 2\delta\Bigg\} \,.\end{aligned} \tag{8}$$

A peak loop is obtained when we keep track of $(E_{\mathrm{peak},n}, P_{\mathrm{peak},n})$ as we vary δ with other parameters

fixed. We present in Fig. 5 the peak loops for the first peak ($n = 0$) obtained from Eqs. (7) and (8) and compare them with the numerical results to confirm a good agreement.

The basic properties of the peak loop are its position, size, and shape, and we quantify them by its central position, width, and height, respectively, as follows. The terms independent of δ in the braces of Eqs. (7) and (8) give the average values of $E_{\mathrm{peak},n}$ and $P_{\mathrm{peak},n}$ over a cycle of δ and can be regarded as the center of a peak loop. The central position up to the first order thus reads

$$\left(\overline{E}_n^{(\pm)}, \overline{P}_n^{(\pm)}\right) = \left(\frac{|\delta m^2_{31}|L}{2\Pi}\left[1 \mp \Delta_{\mathrm{m}}\frac{1}{\Pi}\left(1 - \frac{4}{\Pi^2}\right)(1-2s^2_{13}) \mp Rs^2_{12}\right],\ 4l\left[1 \pm \Delta_{\mathrm{m}}\frac{2}{\Pi}(1-2s^2_{13})\right]\right), \tag{9}$$

where the double sign denotes the same as in Eqs. (7) and (8); see Fig. 6. The terms dependent on δ in Eqs. (7) and (8) account for the size and the shape of a peak loop. The width of a loop $\Delta E_n^{(\pm)}$ and its height $\Delta P_n^{(\pm)}$ can be estimated by taking the difference of the maximum and minimum values of $E_{\mathrm{peak},n}$ and $P_{\mathrm{peak},n}$ as functions of δ (see Fig. 6). They are calculated up to the second order as

$$\Delta E_n^{(\pm)} = |\delta m^2_{31}|LR\frac{1}{\Pi}\sqrt{1+\frac{4}{\Pi^2}}\frac{j}{l}\left[1 \mp \Delta_{\mathrm{m}}\frac{2}{\Pi}\frac{1-32/\Pi^4}{1+4/\Pi^2} \mp R\frac{1}{1+4/\Pi^2}(1-2s^2_{12})\right], \tag{10a}$$

$$\Delta P_n^{(\pm)} = 8R\Pi j\left[1 \pm \Delta_{\mathrm{m}}\frac{2}{\Pi}\left(1-\frac{2}{\Pi^2}\right) \pm Rs^2_{12}\right]. \tag{10b}$$

We notice the numerical magnitude of the correction terms appearing in Eqs. (9) and (10). The correction terms include the matter effect proportional to Δ_{m} and the three-generation effect proportional to R. Of these two, the three-generation effect is even smaller than the matter effect for a typical long baseline experiments. Evaluation using the example values of Eq. (1) is sufficient to verify it by an order-of-magnitude estimation, giving

$$\Delta_{\mathrm{m}}\frac{1}{\Pi} \sim 0.2\left(\frac{L}{1000\,[\mathrm{km}]}\right) \quad \text{for } n = 0\,, \tag{11a}$$

$$R(1-2s^2_{12}) \sim Rs^2_{12} \sim 0.01\,. \tag{11b}$$

The expressions for anti-neutrinos are obtained from Eqs. (9) and (10) by simply flipping the signs of Δ_{m} to give

$$\left(\overline{E}_n^{(\pm)}, \overline{P}_n^{(\pm)}\right) = \left(\frac{|\delta m^2_{31}|L}{2\Pi}\left[1 \pm \Delta_{\mathrm{m}}\frac{1}{\Pi}\left(1 - \frac{4}{\Pi^2}\right)(1-2s^2_{13}) \mp Rs^2_{12}\right],\ 4l\left[1 \mp \Delta_{\mathrm{m}}\frac{2}{\Pi}(1-2s^2_{13})\right]\right), \tag{12}$$

$$\Delta E_n^{(\pm)} = |\delta m^2_{31}|LR\frac{1}{\Pi}\sqrt{1+\frac{4}{\Pi^2}}\frac{j}{l}\left[1 \pm \Delta_{\mathrm{m}}\frac{2}{\Pi}\frac{1-32/\Pi^4}{1+4/\Pi^2} \mp R\frac{1}{1+4/\Pi^2}(1-2s^2_{12})\right], \tag{13a}$$

$$\Delta P_n^{(\pm)} = 8R\Pi j\left[1 \mp \Delta_{\mathrm{m}}\frac{2}{\Pi}\left(1-\frac{2}{\Pi^2}\right) \pm Rs^2_{12}\right]. \tag{13b}$$

Eqs. (12) and (13) have an interesting relation to (9) and (10). The former pair for anti-neutrinos is equivalent to the latter for neutrinos with flipped hierarchy up to the correction terms proportional to Rs^2_{12} or $R(1-2s^2_{12})$, which are small as shown in Eq. (11).

B. Analysis of the peak loops

We elevate the observation of peak loops for neutrinos shown by Fig. 4 in Sec. III B to the systematic analysis applying the formulae we developed in the previous subsection. We also extend our consideration to anti-neutrino case.

Equation (9) reveals the order behind the motion of the loops for neutrinos on the E-P plane as the baseline

length gets longer. The leading dependence of $\overline{E}_n^{(\pm)}$ on the baseline length comes from the prefactor $|\delta m^2_{31}|L/2E$ and drives the loops rightward. Its subleading dependence due to matter-effect term, which is proportional to the baseline length through $\Delta_{\rm m}$ and to $\mathrm{sgn}\,\delta m^2_{31}$, provides a correction which pulls the normal loop back left and gives the inverted loop another push rightward. The other subleading term Rs^2_{12} of $\overline{E}_n^{(\pm)}$ gives an extra correction whose sign depends on the hierarchy and whose magnitude depends on the mass parameters and the mixing parameters but not on the baseline length. The dependence of $\overline{P}_n^{(\pm)}$ on the baseline length is supplied by the matter-effect term which raises the normal loop up and press the inverted loop down. As a whole, a pair of the normal and the inverted loops are driven rightward while they split vertically and their alignment tilts counterclockwise. These features on the motion of the loops are obviously seen in Fig. 4.

We next analyze the distortion of the loop for neutrinos in terms of its width and height given in Eq. (10). The expression of $\Delta E_n^{(\pm)}$ has an overall factor which is proportional to the baseline length and accounts for the widening of the loops. One of two subleading correction of $\Delta E_n^{(\pm)}$ is the matter-effect term which adds the dependence on the baseline length. The other term also gives the correction but does not give any additional dependence on the baseline length. Both of these terms depend on the hierarchy, and counter the widening of the normal loop and augment that of the inverted loop. The dependence of $\Delta P_n^{(\pm)}$ on the baseline length is due to the subleading matter-effect term, which stretches the normal loop and compresses the inverted loop, and the other correction term supplements its effect. All these features of the loops are evident in Fig. 4.

Now that the motion and the distortion of neutrinos are analyzed, those for anti-neutrinos are easy to derive owing to the discussion below Eq. (13) in the previous subsection. A loop for anti-neutrinos moves with distortion just as that for neutrinos with the opposite hierarchy save for the small contribution of the three-generation effect.

The critical baseline length mentioned in the previous section also can be analyzed by our formulation. The critical length is defined as the maximum length giving the intersection of the pairing loops with opposite hierarchies. It is calculated in the first-order approximation as

$$\begin{aligned} L_{\rm crit} =& \frac{1}{\sqrt{2}G_{\rm F}n_{\rm e}}\frac{\Pi}{1-\dfrac{12}{\Pi^2}+\dfrac{64}{\Pi^4}}R\frac{c_{23}c_{12}s_{12}}{s_{13}s_{23}}\frac{1}{1-2s^2_{13}} \\ &\times\left[\sqrt{1-\frac{12}{\Pi^2}+\frac{64}{\Pi^4}-\frac{4}{\Pi^2}\Big(\frac{s_{13}s_{23}s_{12}}{c_{23}c_{12}}\Big)^2}\right. \\ &\left.\mp\Big(1-\frac{8}{\Pi^2}\Big)\frac{s_{13}s_{23}s_{12}}{c_{23}c_{12}}\right]. \end{aligned} \tag{14}$$

where the double sign reads $-$ for neutrinos and $+$ for anti-neutrinos. The prefactor appearing in the right hand side of this expression gives $1/\sqrt{2}G_{\rm F}n_{\rm e} = 5.17\times10^3\,[\mathrm{km}]\cdot(\rho/[\mathrm{g\,cm^{-3}}])^{-1} = 2.0\times10^3\,[\mathrm{km}]\cdot(\rho/[2.6\,\mathrm{g\,cm^{-3}}])^{-1}$. The critical length is inversely proportional to $\sin\theta_{13}$ owing to the factor $c_{23}c_{12}s_{12}/s_{13}s_{23}$, with the small correction of $O(\theta_{13})$. It is particularly important that this dependence can make the critical length very long, since the lower bound on the value of $\sin\theta_{13}$ is unknown at present. Figure 7 shows the dependence of the critical length on $\sin^2 2\theta_{13}$ for the first peak, where other parameters are fixed to the example set of Eq. (1). The critical length for anti-neutrinos is slightly longer than that for neutrinos due to the small correction proportional to $s_{13}s_{23}s_{12}/c_{23}c_{12}$. We quote from this graph $L_{\rm crit} = 1150\,\mathrm{km}$ for neutrinos and $L_{\rm crit} = 1200\,\mathrm{km}$ for anti-neutrinos at $\sin^2 2\theta_{13} = 0.06$. Our results are qualitatively consistent with a similar plot in Ref. [11] for their bi-channel analysis with the energy fixed around a peak at $E = |\delta m^2_{31}|L/2\pi$.

It is remarkable that the following straightforward analysis on the loops reproduces the main part of Eq. (14), which is tedious to derive, and clarifies the origin of the dependence of the critical length upon the mass parameters and the mixing parameters. We compare the separation between the loops with the size of them to obtain a condition for their disentanglement. The separation of the two loops is estimated by the difference between the respective values of $\overline{E}^{(\pm)}$ and $\overline{P}^{(\pm)}$, while the size of each loop is measured by its width and height. We consider the ratio of the separation to the size to compare the two, and define a normalized separation vector as

$$\begin{aligned} &\left(\frac{\overline{E}_n^{(+)}-\overline{E}_n^{(-)}}{\big[\Delta E_n^{(+)}+\Delta E_n^{(-)}\big]/2},\ \frac{\overline{P}_n^{(+)}-\overline{P}_n^{(-)}}{\big[\Delta P_n^{(+)}+\Delta P_n^{(-)}\big]/2}\right) \\ &\simeq \frac{\Delta_{\rm m}}{R}\frac{l}{j}(1-2s^2_{13})\left(-\frac{1}{\Pi}\frac{1-4/\Pi^2}{\sqrt{1+4/\Pi^2}},\ \frac{2}{\Pi^2}\right), \end{aligned} \tag{15}$$

where we neglected the small terms such as Rs^2_{12} and $R(1-s^2_{12})$ in the right-hand side for simplicity. The magnitude of this vector is given by

$$\begin{aligned} S(L) &\simeq \frac{\Delta_{\rm m}}{R}\frac{l}{j}(1-2s^2_{13})\frac{1}{\Pi} \\ &= \frac{\sqrt{2}G_{\rm F}n_{\rm e}}{(2n+1)\pi}L\frac{1}{R}\frac{l}{j}(1-2s^2_{13})\,, \end{aligned} \tag{16}$$

which is proportional to L and parametrizes the configuration of the paired loops, *i.e.* intersected, tangential, or disjoint. The normalization of Eq. (15) is chosen so that the separation at the critical length $S_{\rm crit} \equiv S(L_{\rm crit})$ becomes unity when the loops are two similar ellipses whose major axes are aligned parallel. We write down the critical length from Eq. (16) as

$$L_{\rm crit} = \frac{(2n+1)\pi}{\sqrt{2}G_{\rm F}n_{\rm e}}R\frac{c_{23}c_{12}s_{12}}{s_{23}}\frac{1}{s_{13}}\frac{1}{1-2s^2_{13}}S_{\rm crit}\,. \tag{17}$$

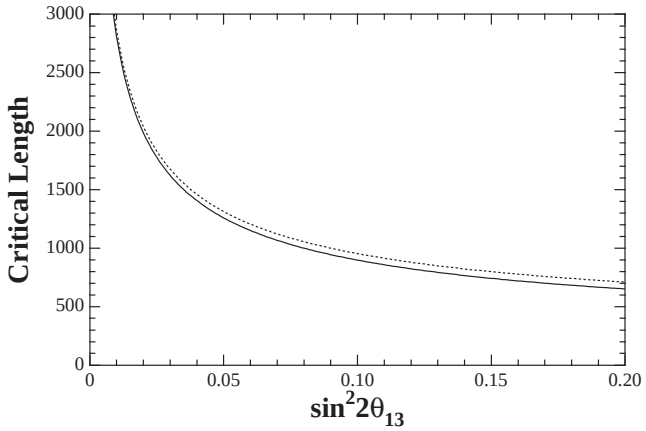

FIG. 7: The critical length as a function of $\sin^2 2\theta_{13}$ calculated by the first-order approximation formula of Eq. (14). The solid line is for neutrinos and the dotted line for anti-neutrinos. The oscillation parameters in Eq. (1) are adopted except for Eq. (1e).

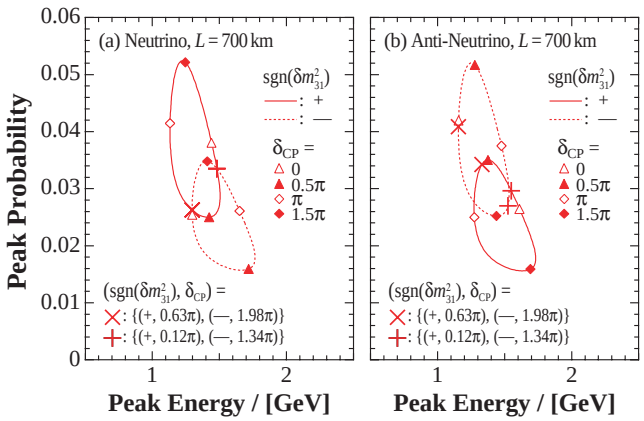

FIG. 8: (Color online) Trajectories of the first peak of (a) $\nu_\mu \to \nu_e$ probability and (b) $\bar{\nu}_\mu \to \bar{\nu}_e$ probability for the baseline length of 700 km. The solid and dotted lines are for the normal and inverted hierarchy, respectively. The cross and the plus sign in (a) are on the intersections of the peak loops, and the corresponding values of parameters are also shown. The signs in (b) mark the points corresponding to these parameter values.

Equation (17) reproduces approximately the same dependence on the parameters as Eq. (14), assuming that $S_{\rm crit}$ does not give any extra dependence on the mass parameters and the mixing parameters.

V. TOWARD THE SOLUTION TO THE HIERARCHY DEGENERACY

In this section, we consider how to escape the hierarchy degeneracy in determining the value of δ by the long baseline experiments.

A promising approach to determining the value of δ and the hierarchy is (1) to do an experiment with baseline length longer than the critical length so that the hierarchy is identified regardless of the value of δ. This lucid approach can be brought into practice by pinning down the position of only one peak. It is nonetheless not free of hurdles: the required baseline length is typically about 1000 km and may be even longer, depending on the value of θ_{13}. Experiments with such a long baseline are challenging due to, for instance, small flux of the neutrino beam and possible large ambiguity of matter effects.

Experiments with shorter baseline are more feasible, but leave the possibility of degeneracy. We can make simultaneous use of two or more peaks to overcome this problem. We examine the effectiveness of the following three approaches of this kind: (2) observing $\bar{\nu}_\mu \to \bar{\nu}_e$ appearance events in addition to $\nu_\mu \to \nu_e$ events; (3) doing two or more experiments with different baseline lengths; and (4) doing an experiment which has more than one oscillation peaks within its visible range of neutrino energy.

The second approach employs both neutrinos and anti-neutrinos. We analyze the benefit of this approach with Fig. 8, which presents two pairs of peak loops, one (a) for neutrinos and the other (b) for anti-neutrinos, with the values of Eq. (1) and $L = 700$ km. The loops in Fig. 8 (a) and (b) resemble each other with opposite assignment of the hierarchy, confirming our discussion in Sec. IV B based on the analytic formulae. Marked by a cross and a plus sign in Fig. 8 (a) are the two intersections of the normal and the inverted loop. Each intersection is associated with two sets of $(\mathrm{sgn}\,\delta m^2_{31}, \delta)$ as we gave examples in Eq. (3) and corresponds to the presence of the hierarchy degeneracy. Turning to Fig. 8 (b), these four parameter sets correspond to four distinct points on the peak loops for anti-neutrinos. Hence the combined analysis of $\nu_\mu \to \nu_e$ events and $\bar{\nu}_\mu \to \bar{\nu}_e$ events will be able to solve the hierarchy degeneracy, provided the two crosses or the two plus signs are distinguishable through experiments. In our present example, the two plus signs for anti-neutrinos are close to each other in the E-P plane and are thus difficult to distinguish. If indistinguishable, the hierarchy degeneracy will persist even with the aid of anti-neutrino events.

The third approach makes use of two or more different baseline lengths [9]. We reproduce in Fig. 9 a series of peak loops shown in Fig. 4. On top of them, we mark the points correspond to the parameter values for the intersections of the loops for $L = 700$ km as we did in Fig. 8. Each pair of loops for a fixed baseline length has two crosses and two plus signs, which reduces, by definition, into a single cross and a single plus sign at $L = 700$ km. The separation between two crosses as well as between two plus signs grows larger as the baseline length deviates from 700 km. The degeneracy on the two crosses or the two plus signs can be thus resolved by

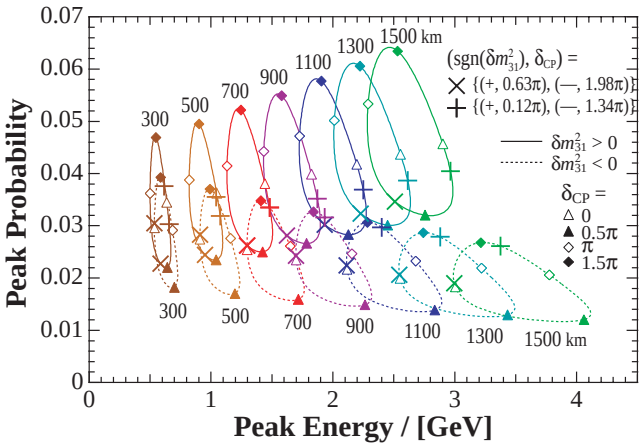

FIG. 9: (Color online) The points correspond to the two sets of parameter values shown in Fig. 8, plotted on top of a series of loops reproduced from Fig. 4. Crosses and plus signs correspond to two intersections of the loops for $L = 700\,\mathrm{km}$. The oscillation parameters in Eq. (1) are adopted. The solid (dotted) line is for the normal (inverted) hierarchy.

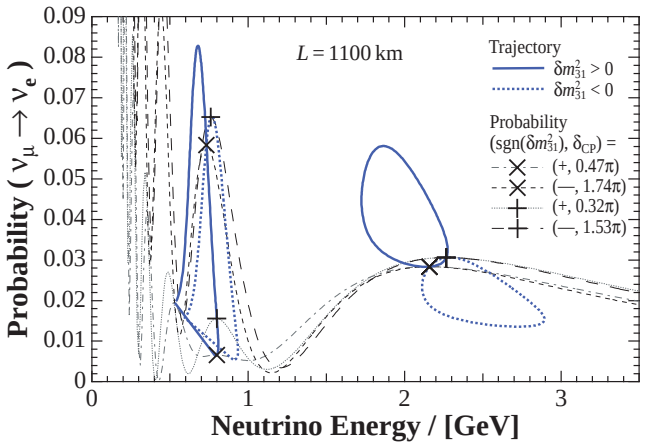

FIG. 10: (Color online) Trajectories of the first and the second oscillation peak for $L = 1100\,\mathrm{km}$. The oscillation parameters in Eq. (1) are adopted. The solid (dotted) loop is for the normal (inverted) hierarchy. Crosses and plus signs correspond to the sets of parameter values that bring the first peak at the intersection of its trajectories. The points for these values are also on the second peak loops and marked by the corresponding sign. Oscillation spectra for the parameter values are overlaid.

an additional experiment with different baseline length, where the large difference of the two baseline lengths is preferable.

The fourth approach exploits other peaks of appearance probability in addition to the first one for $n = 0$ [15]. An analysis covering peaks for different n is effective to solve the degeneracy since each peak has its own properties due to the factor $\Pi \equiv (2n+1)\pi$ in Eqs. (9) and (10). The peak for $n > 0$, however, is not easy to observe due to its small energy which is suppressed by the factor of $1/(2n+1)$. On the other hand, elongation of the baseline length makes peak energies higher, bringing both the first and the second peaks within the range of visible energy. The second-peak loop has different features from the first one, which is effective in solving the degeneracy. We explain the effectiveness by an example shown in Fig. 10, where the baseline length is taken as 1100 km. We show there the two sets of loops traced by the first and second peaks. The second-peak loops are stretched to in the P-direction and have a significant overlap, showing their noticeable difference compared with the first-peak loops. Crosses and plus signs correspond to the values at the two intersections of the loops for the first peak. On the second peak loops, the paired crosses as well as the paired plus signs are separated from each other and are distinguishable by experiments. The hierarchy degeneracy in the first peak will be thereby removed by observing the second peak.

VI. CONCLUSION AND DISCUSSIONS

We studied the search for the leptonic CP-violating angle δ and the neutrino mass hierarchy $\mathrm{sgn}\,\delta m^2_{31}$ by an observation of the $\nu_\mu \to \nu_\mathrm{e}$ oscillation with long baseline experiments. The energy spectrum of $\nu_\mu \to \nu_\mathrm{e}$ appearance probability is engraved with the values of these parameters, although not uniquely. The search for these parameters through the spectrum can lead to degeneracy when the two spectra corresponding to the two different parameter values are indistinguishable. We implemented the presence of degeneracy using the following criterion: the oscillation probabilities for the two parameter values are peaked at the same energy and have the same peak probability. In light of this peak-matching condition, we examined systematically the presence and absence of the degeneracy, especially the hierarchy degeneracy concerning the value of δ and the sign of δm^2_{31}. We have also shown prospects of solving the degeneracy by a single experiment and combinations of experiments.

We introduced a looped trajectory traced by the position of the oscillation peak on the E-P plane while varying the value of δ over $[0, 2\pi]$. We have shown that the loop plays a key rôle in gaining an intuitive view on the parameter degeneracy. We drew pairs of loops for both hierarchies and investigated their properties and behavior to obtain an outlook of the emergence of the hierarchy degeneracy and its resolution. We observed that paired loops with different hierarchies are completely separated when the baseline is longer than the critical length, which is proportional to $1/\sin\theta_{13}$ and is typically about 1000 km or longer. The degeneracy can be avoided in experiments with a sufficiently long baseline length.

With the aid of the peak loops, we obtain a general

view of experimental capabilities to determine the value of δ and the mass hierarchy. We described four ideas for solving the degeneracy by long baseline experiments: taking the baseline longer than the critical length, employing anti-neutrinos as well as neutrinos, using two or more different baseline lengths, and carrying out experiments covering more than one oscillation peaks. We discussed merits and demerits of each idea in terms of the peak loops. We indicated that the first idea of using a sufficiently long baseline is simple but is not free of hurdles. Also pointed out for the second case is that employment of anti-neutrinos does not always solve the degeneracy.

The peak loops we introduced to analyze the parameter degeneracy have an equal versatility to the trajectories in the bi-channel plots presented in Ref. [10]. The two have differences at the same time. One difference is that our plot employs only a single channel and thus can be used for exploring the capabilities of single-channel experiments. Another difference is that we make essential use of the oscillation peak as a representative of the oscillation spectrum over a finite energy range, while the bi-channel plot is drawn for an arbitrary fixed energy or for integrated values over an energy range at one's convenience. The significance of the peak position consists in its implication to the values of the parameters we are in search of. Supported by the peak-matching condition, our method arranges an equipment for a direct prediction of the presence of degeneracy.

We kept the values of the mass parameters and the mixing parameters fixed except for δ and $\mathrm{sgn}\,\delta m^2_{31}$, assuming that these values would be settled in advance of experiments. It is possible, however, that they would not be settled with sufficient precision by that time and that their ambiguities will add another obstacle to the searches [8, 9, 10, 11, 13]. Our peak loops presented in this paper offer an intuitive understanding of effects of these ambiguities also. The position of the oscillation peak in the E-P plane moves around when the value of a parameter is ambiguous and varies within its allowed region. The peak position will be smeared and consequently the loop of the peak will appear broadened and blurred. The value of δ will be accordingly obscured and the mass hierarchy is misidentified within the extended region around the intersection of the loops. Besides, the broadening of a narrow loop makes its paralleling sides indistinguishable. We hence expect that ambiguities of the mass parameters and the mixing parameters worsen the degeneracy of the target parameters and hinder the determination of them. We need extra efforts to hold the ambiguities under control, such as combining with the $\nu_\mu \to \nu_\mu$ disappearance channel or employing reactor neutrino experiments. Detailed analyses of the ambiguities in the framework of the peak loops are left for our future works.

The present analysis based on the peak loops for the oscillation probability is independent of experimental specifications and gives organized understanding of the presence and absence of the degeneracy. More practical evaluation of quantitative capability can be carried out for specific experiments by applying expected number of events to our analysis in place of the oscillation probability. For that purpose, we need to calculate the expected number of events by using a neutrino beam flux of the experiment, the neutrino cross sections, the detector design including a knowledge of systematic errors and backgrounds, and other experimental setups. Drawing the loops traced by the peaks of the spectrum of the event number, we can study a possibility of the presence of degeneracy, estimate quantitatively the allowed region in the parameter space, and select an appropriate baseline length to determine the parameter values.

Acknowledgments

The authors are grateful to Professor Joe Sato for his encouragement during this work.

APPENDIX A: OSCILLATION PROBABILITIES TO THE SECOND ORDER

We calculate the S-matrix of the neutrino oscillation to the second order in $\Delta_{21} \equiv \delta m^2_{21} L/2E$ and $\Delta_{\mathrm{m}} = aL/2E$, and also derive the formula of oscillation probability to this order.

The evolution equation of neutrinos $\nu = (\nu_{\mathrm{e}}, \nu_\mu, \nu_\tau)^{\mathrm{T}}$ is given by

$$\mathrm{i}\frac{\mathrm{d}\nu(x)}{\mathrm{d}x} = H(x)\nu(x)\,, \tag{A1}$$

where

$$H(x) = \frac{1}{2E}\Big(U\,\mathrm{diag}(0, \delta m^2_{21}, \delta m^2_{31})U^\dagger + \mathrm{diag}(a(x), 0, 0)\Big)\,. \tag{A2}$$

Here E is the neutrino energy, U is the unitary mixing matrix of the neutrinos (MNS matrix), and $a(x) = 2\sqrt{2}G_{\mathrm{F}} n_{\mathrm{e}}(x) E$ is the matter effect, where G_{F} is the Fermi constant and $n_{\mathrm{e}}(x)$ is the number density of electrons on the baseline. The probability for a neutrino ν_α to change into ν_β ($\{\alpha, \beta\} \subset \{\mathrm{e}, \mu, \tau\}$) is given by

$$P(\nu_\alpha \to \nu_\beta) = \left|S(x)_{\beta\alpha}\right|^2\,, \tag{A3}$$

where

$$S(x) = \mathrm{T}\exp\left(-\mathrm{i}\int_0^x \mathrm{d}s\, H(s)\right)\,. \tag{A4}$$

We assume in this paper that the spatial variation of the electron density n_{e} is negligible so that Eq. (A4) simplifies to

$$S(x) = \mathrm{e}^{-\mathrm{i}Hx}\,. \tag{A5}$$

We split H as $H = H_0 + H_1$, where

$$H_0 \equiv \frac{1}{2E} U \mathrm{diag}(0, 0, \delta m^2_{31}) U^\dagger \,, \tag{A6}$$

$$H_1 \equiv \frac{1}{2E} \Big(U \mathrm{diag}(0, \delta m^2_{21}, 0) U^\dagger + \mathrm{diag}(a, 0, 0) \Big) \,, \tag{A7}$$

and treat H_1 as a perturbation to obtain

$$S(x) = \mathrm{e}^{-\mathrm{i}H_0 x} \mathrm{T} \exp\left(-\mathrm{i} \int_0^x \mathrm{d}s \, \mathrm{e}^{\mathrm{i}H_0 s} H_1 \mathrm{e}^{-\mathrm{i}H_0 s} \right) . \tag{A8}$$

Expansion of Eq. (A8) leads to a systematic approximation of S-matrix [14]. Explicit calculation of $S(x)$ up to the second order in H_1 shows

$$S(x)_{\beta\alpha} = S_0(x)_{\beta\alpha} + S_1(x)_{\beta\alpha} + S_2(x)_{\beta\alpha} \,, \tag{A9}$$

and

$$S_0(x)_{\beta\alpha} = \delta_{\beta\alpha} - U_{\beta 3} U^*_{\alpha 3} \big(1 - \mathrm{e}^{-\mathrm{i}\Delta_{31}} \big) \,, \tag{A10}$$

$$\begin{aligned} S_1(x)_{\beta\alpha} = & - \mathrm{i}\Delta_{21} U_{\beta 2} U^*_{\alpha 2} \\ & - \mathrm{i}\Delta_{\mathrm{m}} \Big[\delta_{\beta\mathrm{e}} \delta_{\alpha\mathrm{e}} - (\delta_{\alpha\mathrm{e}} + \delta_{\beta\mathrm{e}}) U_{\beta 3} U^*_{\alpha 3} \\ & \quad + |U_{\mathrm{e}3}|^2 U_{\beta 3} U^*_{\alpha 3} \big(1 + \mathrm{e}^{-\mathrm{i}\Delta_{31}} \big) \Big] \\ & - \frac{\Delta_{\mathrm{m}}}{\Delta_{31}} \big(\delta_{\alpha\mathrm{e}} + \delta_{\beta\mathrm{e}} - 2|U_{\mathrm{e}3}|^2 \big) U_{\beta 3} U^*_{\alpha 3} \\ & \quad \times \big(1 - \mathrm{e}^{-\mathrm{i}\Delta_{31}} \big) \,, \end{aligned} \tag{A11}$$

$$\begin{aligned} S_2(x)_{\beta\alpha} = & -\frac{1}{2} \Delta^2_{21} U_{\beta 2} U^*_{\alpha 2} \\ & - \Delta_{\mathrm{m}} \Delta_{21} \left[\frac{1}{2} (\delta_{\alpha\mathrm{e}} + \delta_{\beta\mathrm{e}}) U_{\beta 2} U^*_{\alpha 2} - (U_{\mathrm{e}2} U^*_{\mathrm{e}3} U_{\beta 3} U^*_{\alpha 2} + U_{\mathrm{e}3} U^*_{\mathrm{e}2} U_{\beta 2} U^*_{\alpha 3}) \left(\frac{1}{2} + \frac{\mathrm{i}}{\Delta_{31}} - \frac{1 - \mathrm{e}^{-\mathrm{i}\Delta_{31}}}{\Delta^2_{31}} \right) \right] \\ & - \Delta^2_{\mathrm{m}} \left(\frac{1}{2} \delta_{\beta\mathrm{e}} \delta_{\alpha\mathrm{e}} - (\delta_{\alpha\mathrm{e}} + \delta_{\beta\mathrm{e}}) U_{\beta 3} U^*_{\alpha 3} \left(\frac{1}{2} + \frac{\mathrm{i}}{\Delta_{31}} - \frac{1 - \mathrm{e}^{-\mathrm{i}\Delta_{31}}}{\Delta^2_{31}} \right) \right. \\ & \quad + |U_{\mathrm{e}3}|^2 \left\{ - \delta_{\beta\mathrm{e}} \delta_{\alpha\mathrm{e}} \left(\frac{1}{2} + \frac{\mathrm{i}}{\Delta_{31}} - \frac{1 - \mathrm{e}^{-\mathrm{i}\Delta_{31}}}{\Delta^2_{31}} \right) \right. \\ & \qquad \left. + (1 + \delta_{\alpha\mathrm{e}} + \delta_{\beta\mathrm{e}}) U_{\beta 3} U^*_{\alpha 3} \left[\frac{1}{2} + \frac{\mathrm{i}\big(2 + \mathrm{e}^{-\mathrm{i}\Delta_{31}} \big)}{\Delta_{31}} - \frac{3\big(1 - \mathrm{e}^{-\mathrm{i}\Delta_{31}} \big)}{\Delta^2_{31}} \right] \right\} \\ & \quad \left. - |U_{\mathrm{e}3}|^4 U_{\beta 3} U^*_{\alpha 3} \left[\frac{1 - \mathrm{e}^{-\mathrm{i}\Delta_{31}}}{2} + \frac{3\mathrm{i}\big(1 + \mathrm{e}^{-\mathrm{i}\Delta_{31}} \big)}{\Delta_{31}} - \frac{6\big(1 - \mathrm{e}^{-\mathrm{i}\Delta_{31}} \big)}{\Delta^2_{31}} \right] \right) , \end{aligned} \tag{A12}$$

where $\Delta_{ij} \equiv \delta m^2_{ij} L/2E$ and $\Delta_{\mathrm{m}} \equiv aL/2E$. Substituting Eqs. (A10), (A11) and (A12) into Eq. (A3), we obtain the expression for the oscillation probability up to the second order as

$$P(\nu_\alpha \to \nu_\beta) = p_0(\nu_\alpha \to \nu_\beta) + p_1(\nu_\alpha \to \nu_\beta) + p_2(\nu_\alpha \to \nu_\beta) \,, \tag{A13a}$$

$$p_0(\nu_\alpha \to \nu_\beta) = \delta_{\beta\alpha} - 4|U_{\beta 3}|^2 \big(\delta_{\alpha\beta} - |U_{\alpha 3}|^2 \big) s^2 \,, \tag{A13b}$$

$$\begin{aligned} p_1(\nu_\alpha \to \nu_\beta) = & \, 4\Delta_{21} \Big[\mathrm{Re}\,(U^*_{\beta 3} U_{\beta 2} U_{\alpha 3} U^*_{\alpha 2}) sc - \mathrm{Im}\,(U^*_{\beta 3} U_{\beta 2} U_{\alpha 3} U^*_{\alpha 2}) s^2 \Big] \\ & + 4\Delta_{\mathrm{m}} |U_{\mathrm{e}3}|^2 \big(\delta_{\alpha\mathrm{e}} \delta_{\beta\mathrm{e}} - \delta_{\alpha\mathrm{e}} |U_{\beta 3}|^2 - \delta_{\beta\mathrm{e}} |U_{\alpha 3}|^2 - \delta_{\alpha\beta} |U_{\beta 3}|^2 + 2|U_{\beta 3}|^2 |U_{\alpha 3}|^2 \big) \left(sc - \frac{2}{\Delta_{31}} s^2 \right) , \end{aligned} \tag{A13c}$$

and

$$
\begin{aligned}
p_2(\nu_\alpha \to \nu_\beta) = \Delta_{21}^2 \Big[& -\big(\delta_{\beta\alpha} - |U_{\alpha 2}|^2\big)|U_{\beta 2}|^2 + 2\,\mathrm{Re}\,(U^*_{\beta 3}U_{\beta 2}U_{\alpha 3}U^*_{\alpha 2})s^2 + 2\,\mathrm{Im}\,(U^*_{\beta 3}U_{\beta 2}U_{\alpha 3}U^*_{\alpha 2})sc \Big] \\
& + \Delta_{21}\Delta_{\mathrm{m}} \Bigg\{ -2\big(\delta_{\alpha\mathrm{e}} + \delta_{\beta\mathrm{e}} - 2|U_{\mathrm{e}3}|^2\big)\,\mathrm{Re}\,(U^*_{\beta 3}U_{\beta 2}U_{\alpha 3}U^*_{\alpha 2})\left(1 - s^2 - \frac{2}{\Delta_{31}}sc\right) \\
& \quad + 2\delta_{\alpha\beta}\,\mathrm{Re}\,(U^*_{\beta 3}U_{\beta 2}U_{\mathrm{e}3}U^*_{\mathrm{e}2})\left(1 - \frac{4}{\Delta_{31}^2}s^2\right) \\
& \quad - 2\Big[|U_{\beta 3}|^2\,\mathrm{Re}\,(U^*_{\mathrm{e}3}U_{\mathrm{e}2}U_{\alpha 3}U^*_{\alpha 2}) + |U_{\alpha 3}|^2\,\mathrm{Re}\,(U^*_{\beta 3}U_{\beta 2}U_{\mathrm{e}3}U^*_{\mathrm{e}2})\Big]\left(s^2 + \frac{2}{\Delta_{31}}sc - \frac{4}{\Delta_{31}^2}s^2\right) \\
& \quad - 2\Big[|U_{\beta 3}|^2\,\mathrm{Im}\,(U^*_{\mathrm{e}3}U_{\mathrm{e}2}U_{\alpha 3}U^*_{\alpha 2}) + |U_{\alpha 3}|^2\,\mathrm{Im}\,(U^*_{\beta 3}U_{\beta 2}U_{\mathrm{e}3}U^*_{\mathrm{e}2}) \\
& \qquad - \big(\delta_{\alpha\mathrm{e}} + \delta_{\beta\mathrm{e}} - 2|U_{\mathrm{e}3}|^2\big)\,\mathrm{Im}\,(U^*_{\beta 3}U_{\beta 2}U_{\alpha 3}U^*_{\alpha 2})\Big]\left(sc - \frac{2}{\Delta_{31}}s^2\right)\Bigg\} \\
& + \Delta_{\mathrm{m}}^2 \Bigg\{ -|U_{\mathrm{e}3}|^2\big(\delta_{\alpha\mathrm{e}}\delta_{\beta\mathrm{e}} - \delta_{\alpha\mathrm{e}}|U_{\beta 3}|^2 - \delta_{\beta\mathrm{e}}|U_{\alpha 3}|^2\big)\left(1 - 2s^2 - \frac{8}{\Delta_{31}}sc + \frac{12}{\Delta_{31}^2}s^2\right) \\
& \quad - \delta_{\alpha\beta}|U_{\mathrm{e}3}|^2|U_{\beta 3}|^2\left(1 + \frac{4}{\Delta_{31}}sc - \frac{12}{\Delta_{31}^2}s^2\right) \\
& \quad + 2|U_{\mathrm{e}3}|^2|U_{\beta 3}|^2|U_{\alpha 3}|^2\left(s^2 + \frac{6}{\Delta_{31}}sc - \frac{12}{\Delta_{31}^2}s^2\right) \\
& \quad + 2\delta_{\alpha\beta}|U_{\mathrm{e}3}|^4|U_{\beta 3}|^2\left(s^2 + \frac{6}{\Delta_{31}}sc - \frac{12}{\Delta_{31}^2}s^2\right) \\
& \quad + |U_{\mathrm{e}3}|^4\big(\delta_{\alpha\mathrm{e}}\delta_{\beta\mathrm{e}} - \delta_{\alpha\mathrm{e}}|U_{\beta 3}|^2 - \delta_{\beta\mathrm{e}}|U_{\alpha 3}|^2\big)\left(4 - 6s^2 - \frac{28}{\Delta_{31}}sc + \frac{40}{\Delta_{31}^2}s^2\right) \\
& \quad + 4|U_{\mathrm{e}3}|^4|U_{\beta 3}|^2|U_{\alpha 3}|^2\left(1 - 2s^2 - \frac{10}{\Delta_{31}}sc + \frac{16}{\Delta_{31}^2}s^2\right)\Bigg\},
\end{aligned}
\tag{A13d}
$$

in which we used abbreviations of $s = \sin(\Delta_{31}/2)$ and $c \equiv \cos(\Delta_{31}/2)$. This lengthy expression of Eq. (A13) has the form of

$$
\begin{aligned}
P(\nu_\alpha \to \nu_\beta) = & C_1 \sin^2\frac{\Delta_{31}}{2} + C_2 \sin\frac{\Delta_{31}}{2}\cos\frac{\Delta_{31}}{2} \\
& + C_3\,,
\end{aligned}
\tag{A14}
$$

where the coefficients C_1, C_2, and C_3 are written in terms of the elements of the mixing matrix, the mass parameters, and Δ_{m}. The coefficient C_1 is of $O(1)$ while C_2 and C_3 are of the first-order or higher, so that Eq. (A14) reduces to the two-generation formula in the zeroth-order approximation. We factor out $\sin(\Delta_{31}/2)$ from the sum of sinusoidal functions and transform the sum of sine and cosine into a single sine as

$$
\begin{aligned}
& P(\nu_\alpha \to \nu_\beta) \\
& = \sqrt{C_1^2 + C_2^2}\,\sin\frac{\Delta_{31}}{2}\sin\left(\frac{\Delta_{31}}{2} + C_4\right) + C_3\,,
\end{aligned}
\tag{A15}
$$

where $C_4 = \arctan(C_2/C_1)$. We rewrite Eq. (A15) as

$$
\begin{aligned}
P(\nu_\alpha \to \nu_\beta) = & \sqrt{C_1^2 + C_2^2}\,\sin^2\left(\frac{\Delta_{31}}{2} + \frac{C_4}{2}\right) \\
& - \sqrt{C_1^2 + C_2^2}\,\sin^2\frac{C_4}{2} + C_3\,,
\end{aligned}
\tag{A16}
$$

which reproduces the form of Eq. (4a) with

$$
A \equiv \frac{1}{4l}\sqrt{C_1^2 + C_2^2}\,, \tag{A17a}
$$

$$
\Theta \equiv \frac{\Delta_{31}}{2} + \frac{C_4}{2}\,, \tag{A17b}
$$

$$
B \equiv \frac{1}{4l}\left(C_3 - \sqrt{C_1^2 + C_2^2}\,\sin^2\frac{C_4}{2}\right). \tag{A17c}
$$

The expressions of Eqs. (4b), (4c), and (4d) are obtained from Eq. (A17) by setting $\alpha = \mu$ and $\beta = \mathrm{e}$ within C_1, C_2, C_3, and C_4 and taking up to the appropriate order.

APPENDIX B: VALIDITY OF THE APPROXIMATION

We made use of an approximated formulae of the oscillation probability in Sec. IV. We assemble the requirements for the these formulae to be valid.

The approximation we developed in Appendix A requires

$$\delta m^2_{31} \gg a, \delta m^2_{21}\,, \tag{B1}$$

$$\Delta_{\rm m} \equiv \frac{aL}{2E} = 5.0\times10^{-1}\left(\frac{L}{1000\,[{\rm km}]}\right)\left(\frac{\rho}{2.6\,[{\rm g\,cm^{-3}}]}\right) \ll 1\,, \tag{B2}$$

and

$$\Delta_{21}(E) \equiv \frac{\delta m^2_{21}L}{2E} = 2.1\times10^{-1}\left(\frac{\delta m^2_{21}}{8.2\cdot10^{-5}[{\rm eV}^2]}\right)\left(\frac{L}{1000\,[{\rm km}]}\right)\left(\frac{E}{[{\rm GeV}]}\right)^{-1} \ll 1. \tag{B3}$$

Since neutrino energy we consider in this paper is $E \approx E_{{\rm peak},n} \approx |\delta m^2_{31}|L/[2(2n+1)\pi]$, the conditions of Eqs. (B) are satisfied at least marginally for $L \sim (300-1500)$km.

We additionally simplified the expression by dropping higher-order terms of $\sin\theta_{13}$ taking account of its smallness as we mentioned in Sec. IV. Taking $\Delta_{21} < \Delta_{\rm m}$ into account, we dropped terms of $O(\sin^2\theta_{13})$ in the coefficients of Δ^2_{21} and of $\Delta_{21}\Delta_{\rm m}$ as well as terms of $O(\sin^3\theta_{13})$ in the coefficients of $\Delta^2_{\rm m}$. This simplification is valid when the neglected terms are much smaller than the leading term which is of $O(\sin^2\theta_{13})$, namely

$$\frac{\Delta_{21}(E_{{\rm peak},n})^2\sin^2\theta_{13}}{\sin^2\theta_{13}} = 1.1\times10^{-2}\cdot(2n+1)^2\frac{\left(\frac{\delta m^2_{21}}{8.2\cdot10^{-5}\,[{\rm eV}^2]}\right)^2}{\left(\frac{|\delta m^2_{31}|}{2.5\cdot10^{-3}\,[{\rm eV}^2]}\right)^2} \ll 1\,, \tag{B4}$$

$$\frac{\Delta_{21}(E_{{\rm peak},n})\Delta_{\rm m}\sin^2\theta_{13}}{\sin^2\theta_{13}} = 5.2\times10^{-2}\cdot(2n+1)\frac{\left(\frac{\delta m^2_{21}}{8.2\cdot10^{-5}\,[{\rm eV}^2]}\right)}{\left(\frac{|\delta m^2_{31}|}{2.5\cdot10^{-3}\,[{\rm eV}^2]}\right)}\left(\frac{L}{1000\,[{\rm km}]}\right)\left(\frac{\rho}{2.6\,[{\rm g\,cm^{-3}}]}\right) \ll 1\,, \tag{B5}$$

and

$$\frac{\Delta^2_{\rm m}\sin^3\theta_{13}}{\sin^2\theta_{13}} = 2.5\times10^{-1}\cdot\sin\theta_{13}\left(\frac{L}{1000\,[{\rm km}]}\right)^2\left(\frac{\rho}{2.6\,[{\rm g\,cm^{-3}}]}\right)^2 \ll 1. \tag{B6}$$

These inequalities are well satisfied for allowed value of $\sin^2 2\theta_{13} < 0.19$ [5].

[1] B. T. Cleveland *et al.*, Astrophys. J. **496**, 505 (1998); Y. Fukuda *et al.* [Kamiokande Collaboration], Phys. Rev. Lett. **77**, 1683 (1996); J. N. Abdurashitov *et al.* [SAGE Collaboration], J. Exp. Theor. Phys. **95**, 181 (2002) [Zh. Eksp. Teor. Fiz. **122**, 211 (2002)]; W. Hampel *et al.* [GALLEX Collaboration], Phys. Lett. B **447**, 127 (1999); M. Altmann *et al.* [GNO Collaboration], Phys. Lett. B **616**, 174 (2005); M. B. Smy *et al.* [Super-Kamiokande Collaboration], Phys. Rev. D **69**, 011104 (2004); S. N. Ahmed *et al.* [SNO Collaboration], Phys. Rev. Lett. **92**, 181301 (2004); B. Aharmim *et al.* [SNO Collaboration], Phys. Rev. C **72**, 055502 (2005).

[2] Y. Ashie *et al.* [Super-Kamiokande Collaboration], Phys. Rev. Lett. **93**, 101801 (2004); Y. Ashie *et al.* [Super-Kamiokande Collaboration], Phys. Rev. D **71**, 112005 (2005); M. C. Sanchez *et al.* [Soudan 2 Collaboration], Phys. Rev. D **68**, 113004 (2003); M. Ambrosio *et al.* [MACRO Collaboration], Eur. Phys. J. C **36**, 323 (2004).

[3] T. Araki *et al.* [KamLAND Collaboration], Phys. Rev. Lett. **94**, 081801 (2005); E. Aliu *et al.* [K2K Collaboration], Phys. Rev. Lett. **94**, 081802 (2005).

[4] M. Apollonio *et al.* [CHOOZ Collaboration], Eur. Phys.

J. C **27**, 331 (2003).
[5] W. M. Yao *et al.* [Particle Data Group], J. Phys. G **33**, 1 (2006).
[6] F. Ardellier *et al.*, arXiv:hep-ex/0405032; J. Cao, Nucl. Phys. Proc. Suppl. **155**, 229 (2006); M. Aoki *et al.*, arXiv:hep-ex/0607013.
[7] Y. Itow *et al.*, KEK report 2001-4, ICRR-report-477-2001-7, TRI-PP-01-05 [arXiv:hep-ex/0106019]. D. S. Ayres *et al.* [NOvA Collaboration], Fermilab-Proposal-0929 [arXiv:hep-ex/0503053].
[8] A. Cervera, A. Donini, M. B. Gavela, J. J. Gómez Cadenas, P. Hernández, O. Mena, and S. Rigolin, Nucl. Phys. B **579**, 17 (2000) [Erratum-ibid. B **593**, 731 (2001)]; M. Koike, T. Ota, and J. Sato, Phys. Rev. D **65**, 053015 (2002); J. Burguet-Castell, M. B. Gavela, J. J. Gómez Cadenas, P. Hernández, and O. Mena, Nucl. Phys. B **608**, 301 (2001); M. Freund, P. Huber, and M. Lindner, Nucl. Phys. B **615**, 331 (2001); J. Pinney and O. Yasuda, Phys. Rev. D **64**, 093008 (2001); P. Huber, M. Lindner, and W. Winter, Nucl. Phys. B **645**, 3 (2002); H. Minakata, H. Nunokawa, and S. J. Parke, Phys. Rev. D **66**, 093012 (2002); J. Burguet-Castell, M. B. Gavela, J. J. Gómez Cadenas, P. Hernández, and O. Mena, Nucl. Phys. B **646**, 301 (2002); P. Huber, M. Lindner, M. Rolinec, T. Schwetz and W. Winter, Phys. Rev. D **70**, 073014 (2004); O. Mena and S. J. Parke, Phys. Rev. D **70**, 093011 (2004); A. Donini, E. Fernandez-Martinez, and S. Rigolin, Phys. Lett. B **621**, 276 (2005); P. Huber, M. Lindner, and W. Winter, JHEP **0505**, 020 (2005); P. Huber, M. Maltoni, and T. Schwetz, Phys. Rev. D **71**, 053006 (2005).
[9] Y. F. Wang, K. Whisnant, Z. h. Xiong, J. M. Yang and B. L. Young [VLBL Study Group H2B-4], Phys. Rev. D **65**, 073021 (2002); M. Aoki, K. Hagiwara, Y. Hayato, T. Kobayashi, T. Nakaya, K. Nishikawa and N. Okamura, Phys. Rev. D **67**, 093004 (2003); K. Whisnant, J. M. Yang and B. L. Young, Phys. Rev. D **67**, 013004 (2003); V. Barger, D. Marfatia, and K. Whisnant, Phys. Lett. B **560**, 75 (2003); M. Ishitsuka, T. Kajita, H. Minakata, and H. Nunokawa, Phys. Rev. D **72**, 033003 (2005); K. Hagiwara, N. Okamura, and K. i. Senda, Phys. Lett. B **637**, 266 (2006) [Erratum-ibid. B **641**, 491 (2006)]; T. Kajita, H. Minakata, S. Nakayama, and H. Nunokawa, Phys. Rev. D **75**, 013006 (2007).
[10] H. Minakata and H. Nunokawa, JHEP **0110**, 001 (2001); H. Minakata, H. Nunokawa and S. J. Parke, Phys. Lett. B **537**, 249 (2002).
[11] V. Barger, D. Marfatia, and K. Whisnant, Phys. Rev. D **65**, 073023 (2002).
[12] A. Aguilar *et al.* [LSND Collaboration], Phys. Rev. D **64**, 112007 (2001).
[13] M. Koike, N. Okamura, M. Saito, and T. Takeuchi, Phys. Rev. D **73**, 053010 (2006).
[14] J. Arafune, M. Koike, and J. Sato, Phys. Rev. D **56**, 3093 (1997) [Erratum-ibid. D **60**, 119905 (1999)]; M. Koike and J. Sato, Mod. Phys. Lett. A **14**, 1297 (1999); M. Koike and J. Sato, Phys. Rev. D **61**, 073012 (2000) [Erratum-ibid. D **62**, 079903 (2000)].
[15] M. V. Diwan *et al.*, Phys. Rev. D **68**, 012002 (2003).